applied optics

Optimal design of tilt carrier frequency computer-generated holograms to measure aspherics

Jiantao Peng,[1,2,*] Zhe Chen,[1,2] Xingxiang Zhang,[1] Tianjiao Fu,[1,2] and Jianyue Ren[1]

[1]Changchun Institute of Optics, Fine Mechanics and Physics, Chinese Academy of Science, Changchun 130033, China
[2]University of Chinese Academy of Sciences, Beijing 100049, China
*Corresponding author: jtpeng1989@163.com

Received 15 May 2015; revised 15 July 2015; accepted 21 July 2015; posted 28 July 2015 (Doc. ID 241063); published 19 August 2015

Computer-generated holograms (CGHs) provide an approach to high-precision metrology of aspherics. A CGH is designed under the trade-off among size, mapping distortion, and line spacing. This paper describes an optimal design method based on the parametric model for tilt carrier frequency CGHs placed outside the interferometer focus points. Under the condition of retaining an admissible size and a tolerable mapping distortion, the optimal design method has two advantages: (1) separating the parasitic diffraction orders to improve the contrast of the interferograms and (2) achieving the largest line spacing to minimize sensitivity to fabrication errors. This optimal design method is applicable to common concave aspherical surfaces and illustrated with CGH design examples.

OCIS codes: (090.1760) Computer holography; (050.1970) Diffractive optics; (120.4630) Optical inspection; (220.1250) Aspherics.

http://dx.doi.org/10.1364/AO.54.007433

1. INTRODUCTION

Optical testing using computer-generated holograms (CGHs) has become a standard practice in high-precision measurements of aspherical surfaces [1–3]. Separating the parasitic diffraction orders [4], enlarging the line spacing [5], reducing the size, and controlling the mapping distortion [6] are the key problems for CGHs design, where the size and the mapping distortion are usually weighed and fixed at the beginning of the design.

The parasitic diffraction orders of a CGH along with the desired measurement order reduce the overall quality of the interferograms, unless all the disturbing orders are filtered out. Tilt or power carrier frequency is applied to a CGH to separate the diffraction orders [7,8]. However, for the CGH placed outside the interferometer focus point, because of the multiple diffraction order combinations, it is complex to find the solution for the needed amount of carrier frequency, which is usually attained with the inefficient method of trial and error [9].

CGH patterns are made with a common range of the line spacing from 5 to 30 μm, owing to the widespread usage of the semiconductor technologies [10]. A CGH with small line spacing risks inaccuracy caused by manufacturing errors and even the limitation of scalar diffraction theory if the local line spacing is less than 2.85 μm [5]. The line spacing of a CGH will be shortened when carrier frequency is adopted. Therefore, the least carrier frequency is pursued to maximize the line spacing.

For CGHs placed outside the interferometer focuses, some work has been done to probe the disturbing effects of the multiple diffraction orders and the needed amount of carrier frequency to spatially isolate the desired order. Lindlein [11] derived an approximate expression for the spatial frequencies of the undesired diffraction orders when the CGH is close to the test mirror. Garbusi and Osten [12] analyzed the influence of the unwanted orders that impinge defocused on the interferometer's inner filtering aperture. Zhou *et al.* [9] obtained a paraxial solution for the amount of carrier frequency needed for the CGHs with power carriers. In our previous work [13], we constructed a paraxial parametric model and achieved a recipe for determining the amount of tilt carrier frequency, which is applicable to concave weak aspheric surfaces with large f-numbers.

As an extension of our previous work on the tilt carrier frequency CGHs placed outside the interferometer focus points, the purpose of this paper is (1) to expand the application range of the parametric model and (2) to approach the largest line spacing when the upper limits of the size and the mapping distortion are specified. In this paper, concave aspherical surfaces with the conic constant K of $-4 \le K < 0$ and the f-numbers of $F/\# \ge 1.5$ are considered. No paraxial approximation is applied, and all the expressions are represented with respect to the mirror coordinate and approximated up to seventh order to upgrade the precision and hence the application range of the parametric model. Merit functions are proposed to search for the most appropriate design to achieve the largest line spacing. In Section 2, the representative diffraction orders (2, 0) and (1, 0) are concentrated on to derive the condition for separating the parasitic orders. In Section 3, the influence of the conic constant K, the $F/\#$, the relative position between the CGH

and the pinhole, and the CGH glass plate on the separated distances of the orders (2, 0) and (1, 0) is discussed. In Section 4, the optimal design method of eliminating the parasitic orders and achieving the largest line spacing is displayed in detail. In Section 5, CGH design examples are exhibited.

2. PARAMETRIC MODEL

A. CGH Size and Mapping Distortion

The parametric model constructed in our previous work is applied to analyze the parasitic diffraction orders of tilt carrier frequency CGHs [13]. A thin CGH placed outside the interferometer focus converts a standard spherical wavefront into an aspheric wavefront that matches the test mirror (Fig. 1). The phase function of the CGH is fully determined by the test mirror, the distance h between the CGH and the paraxial focus C, and the axial distance p and the transverse distance t between the CGH and the pinhole.

If the aperture of the interferometer is parallel to the CGH, and the distortion caused by the interferometer and the CGH glass plate is insignificant, the CGH mapping distortion can be described by the relation between the CGH coordinate (x, y) and the mirror coordinate (ξ, η). It can be approximated up to seventh order as

$$r \approx \frac{h}{R} r_m + \frac{(K+1)h - KR}{2R^3} r_m^3 + \frac{3(K+1)((K+1)h - KR)}{8R^5} r_m^5 + \frac{5(K+1)^2((K+1)h - KR)}{16R^7} r_m^7, \quad (1)$$

where R is the radius of curvature, K is the conic constant, and $r = (x^2 + y^2)^{1/2}$ and $r_m = (\xi^2 + \eta^2)^{1/2}$ are the radial position on the CGH and the conic surface, respectively.

The nonlinearity of Eq. (1) determines the mapping distortion, and the greatest value of Eq. (1) determines the size of the CGH (main CGH section). It demonstrates that the size and the mapping distortion are fully determined by the distance h between the CGH and the paraxial focus.

B. Separated Distances of Undesired Diffraction Orders

In order to expand its application range, the precision of the parametric model must be improved. Therefore, no paraxial approximation is allowed. Simultaneously, we describe all the expressions with respect to the mirror coordinate (ξ, η) to avert the error caused by the transformation from the CGH coordinate (x, y) to mirror coordinate (ξ, η), since the high-precision rational expression of $(\xi, \eta) = f(x, y)$, i.e., the inverse function of Eq. (1), is hard to obtain for the high nonlinearity of Eq. (1), while the iterative method cannot attain the analytical expression.

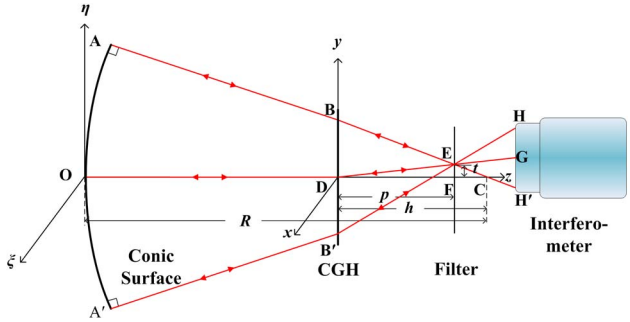

Fig. 1. Schematic of the parametric geometric model for the optical testing of a conic surface with a curvature radius R. Point C is the paraxial focus of the test mirror. Point E is the focus point of the interferometer. The parameters h, p, and t are defined as shown.

The spherical wave from the interferometer passes through the CGH twice and is divided into different diffraction orders. Among the multiple diffraction order combinations (m, n), where m is the order during the first passage of the CGH and n is the order during the second, we focus on the orders (2, 0) and (1, 0) to analyze the disturbing field on the filter plane based on the following reasons:

(1) The entire unwanted diffraction orders (m, n) can be classified into the orders (m, n), with $m + n - 2 = 0$ and $(m - 1)(n - 1) = 0$, and $(m + n - 2)(m - 1)(n - 1) \neq 0$, according to the paraxial expression for the detached distance $\Delta l_{(m,n)}(y)$ of the order (m, n) (on the meridional plane) [13],

$$\Delta l_{(m,n)}(y) = (m + n - 2)p\frac{\partial \Phi}{\partial y} + 2(m - 1)(n - 1)ph\frac{R - h}{R}\frac{\partial \Phi}{\partial y}\frac{\partial^2 \Phi}{\partial y^2}, \quad (2)$$

where Φ is the phase function of the CGH. Herein, for simplicity, not the optical path difference (OPD) multiplied by the wave vector but the OPD itself is used to describe the phase function.

(2) The orders (2, 0) and (0, 2) can be chosen as the representative of the orders (m, n) with $m + n - 2 = 0$, as the latter are approximately $|(m - 1)(n - 1)|$ times the separated distances of the former two. This has been shown by Eq. (2) and verified in our previous work.

(3) The orders (1, 0) and (0, 1) are considered and treated as the representative of the diffraction orders (m, n) with $(m - 1)(n - 1) = 0$.

(4) Lindlein and our previous work have shown the quasi-symmetry between the orders (m, n) and (n, m) [11,13].

(5) The orders (2, 0) and (1, 0), instead of the orders (0, 2) and (0, 1), are concentrated on to avoid the transformation from the CGH coordinate (x, y) to the mirror coordinate (ξ, η).

(6) Although the orders (m, n) with $(m + n - 2)(m - 1)(n - 1) \neq 0$ are not represented, the orders (2, 0) and (1, 0) are enough to analyze most of them. This will be explained in detail in Section 3.

The propagation of the diffraction order $(m, 0)$, where $m =$ 1 or 2, is shown in Fig. 2. Rays on the meridional plane are analyzed. The separated distance $\Delta l_{(m,0)}(\eta)$ of the order $(m, 0)$, indicated as the distance EE', is calculated as follows:

(a) The ray PA is perpendicular to the test mirror. The point P $(0, y)$ is fully determined by the point A $(0, \eta)$ as Eq. (1).

(b) The local surface normal vector $\mathbf{N}$ is written as $(0, N_y, N_z)$, where $N_z = (1 - N_y^2)^{1/2}$ and

$$N_y(\eta) \approx -\frac{\eta}{R} - \frac{K\eta^3}{2R^3} - \frac{3K^2\eta^5}{8R^5} - \frac{5K^3\eta^7}{16R^7}. \quad (3)$$

(c) According to the vector diffraction equation of CGHs [14], the angles ψ, θ_1 and θ_m have the relationship

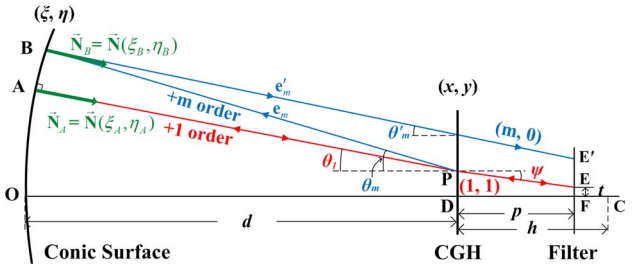

Fig. 2. Propagation of the disturbing order $(m, 0)$ and the desired one $(1, 1)$. $d = R - h$. $\mathbf{N}$ ($\mathbf{N}_A$ and $\mathbf{N}_B$) is the local surface normal vector. $\mathbf{e}_m$ and $\mathbf{e}'_m$ are the direction vectors. The vectors $\mathbf{N}$, $\mathbf{e}_m$, and $\mathbf{e}'_m$ are normalized. ψ, θ_1, θ_m, and θ'_m are the incidence/emergence angles as shown. EE' is the separated distance of the order $(m, 0)$.

$$\frac{\partial \Phi}{\partial y} = \sin\theta_1 - \sin\psi,\ m\frac{\partial \Phi}{\partial y} = \sin\theta_m - \sin\psi, \tag{4}$$

where

$$\sin\theta_1 = -N_y(\eta), \qquad \sin\psi = \frac{y - t}{\sqrt{p^2 + (y - t)^2}}. \tag{5}$$

(d) The coordinate of point B is approximated as $(0, \eta_B, \eta_B^2/2R)$. Thus, we obtain

$$\eta_B - y = \left(d - \frac{\eta_B^2}{2R}\right)\tan\theta_m,$$

$$\eta_B \approx (d\tan\theta_m + y) - \frac{\tan\theta_m}{2R}(d\tan\theta_m + y)^2 + \frac{\tan^2\theta_m}{2R^2}(d\tan\theta_m + y)^3. \tag{6}$$

(e) In accordance with the vector equation of reflection law, the direction vector $\mathbf{e}'_m = (0, -\sin\theta'_m, \cos\theta'_m)$ is obtained as

$$\mathbf{e}'_m = \mathbf{e}_m - 2(\mathbf{e}_m \cdot \mathbf{N}_B)\mathbf{N}_B \approx \mathbf{e}_m + 2\mathbf{N}_B,$$
$$-\sin\theta'_m \approx \sin\theta_m + 2N_{By} = \sin\theta_m + 2N_y(\eta_B), \tag{7}$$

where $\mathbf{N}_B = \mathbf{N}(\xi_B, \eta_B)$, shown in Fig. 2, and the approximation $\mathbf{e}_m \cdot \mathbf{N}_B \approx -1$ is adopted, based on the fact that the included angle between $\mathbf{e}_m$ and $\mathbf{N}_B$ is nearly 180°.

(f) The separated distance EE' is calculated as

$$\Delta l_{(m,0)}(\eta) = \eta_B + \left(d + p - \frac{\eta_B^2}{2R}\right)(-\tan\theta'_m) - t. \tag{8}$$

(g) With Eq. (1) and Eqs. (3)–(8) and the relation $\tan\theta = \sin\theta/(1 - \sin^2\theta)^{1/2}$, the expression of $\Delta l_{(m,0)}(\eta)$ is fully obtained.

However, the whole expression of $\Delta l_{(m,0)}(\eta)$ is too complicated to show here unless $m = 1$, in which case $\Delta l_{(m,0)}(\eta)$ is simplified to

$$\Delta l_{(1,0)}(\eta) = -t + \frac{h - p}{R}\eta + ((K + 1)(h - p) - KR) \times \left(\frac{1}{2R^3}\eta^3 + \frac{3(K + 1)}{8R^5}\eta^5 + \frac{5(K + 1)^2}{16R^5}\eta^7\right). \tag{9}$$

C. Condition for Separating the Parasitic Diffraction Orders

A pinhole is applied to block off the stray rays away from the interferometer focus E (Fig. 1). Owing to the practical precision of fabrication and alignment of the pinhole, a necessary separated distance L_0 is adopted as a criterion. Thus, the condition for separating the parasitic diffraction orders is

$$|\Delta l_{(m,0)}(\eta)| \geq L_0. \tag{10}$$

Note that there is a relationship in accordance with the dimensional analysis

$$\Delta l_{(m,0)}(\alpha\eta, \alpha R, \alpha h, \alpha p, \alpha t, K, F/\#) = \alpha \cdot \Delta l_{(m,0)}(\eta, R, h, p, t, K, F/\#), \tag{11}$$

where α is a scaling factor.

D. Extended to Concave Surfaces with Aspheric Coefficients

When a conic surface with fourth-, sixth-, and eighth-order coefficients describing the asphericity is under test, the derivation of the separated distance $\Delta l_{(m,0)}(\eta)$ is similar except that

$$r \approx \frac{h}{R}r_m + \frac{(K + a + 1)h - (K + a)R}{2R^3}r_m^3 + \{3[(1 + K)^2 + b]h - 3[K(K + 1) - a + b]R\}\frac{r_m^5}{8R^5} + \{5[(K + 1)^3 + c]h - [5(K(K + 1)^2 + c) - 2(K + 1)a - a^2 - 4b]R\}\frac{r_m^7}{16R^7},$$
$$N_y(\eta) = -\frac{\eta}{R} - \frac{(K + a)\eta^3}{2R^3} - \frac{3(K^2 - 2a + b)\eta^5}{8R^5} - \frac{(5K^3 - 12Ka - 6a^2 + 3a - 9b + 5c)\eta^7}{16R^7}, \tag{12}$$

with

$$a = 8AR^3, \qquad b = 16BR^5, \qquad c = 128CR^7/5, \tag{13}$$

where A, B, and C are the fourth-, sixth-, and eighth-order coefficients, respectively. Note that in this case, the separated distance $\Delta l_{(1,0)}(\eta)$ is no longer described as Eq. (9).

3. DISCUSSION

A. Influence of $F/\#$, Conic Constant K, and Parameters p and t

Previous work [13] proposed a paraxial analytical solution which possesses high precision when $-0.5 \leq K < 0$ and $F/\# \geq 2$ ($F/\#$ is defined as $R/2D$, where D is the aperture of the test mirror). In order to expand the application range of the parametric model, the influence of the $F/\#$ and the conic constant K is discussed at first. The separated distance $\Delta l_{(m,0)}(\eta)$ versus the $F/\#$ and the conic constant K is shown in Fig. 3. The calculated $\Delta l_{(m,0)}(\eta)$ matches the Zemax-based ray trace well, which verifies the rationality of the approximation made in Section 2. Results show that the function $\Delta l_{(m,0)}(\eta)$ is highly nonlinear when the absolute value of K is large and $F/\#$ is small, implying that in this case an approximate expression of $\Delta l_{(m,0)}(\eta)$ up to low order (e.g., fourth order in our previous work) is inaccurate. That is one of the reasons why our previous work is only applicable when $-0.5 \leq K < 0$ and $F/\# \geq 2$.

The plots from Figs. 4 and 5 give the separated distance $\Delta l_{(m,0)}(\eta)$ of the order $(m, 0)$, where $m = 1$ or 2, versus the variations of the axial distance p and the transverse distance t between the CGH and the pinhole. Figure 4 shows that

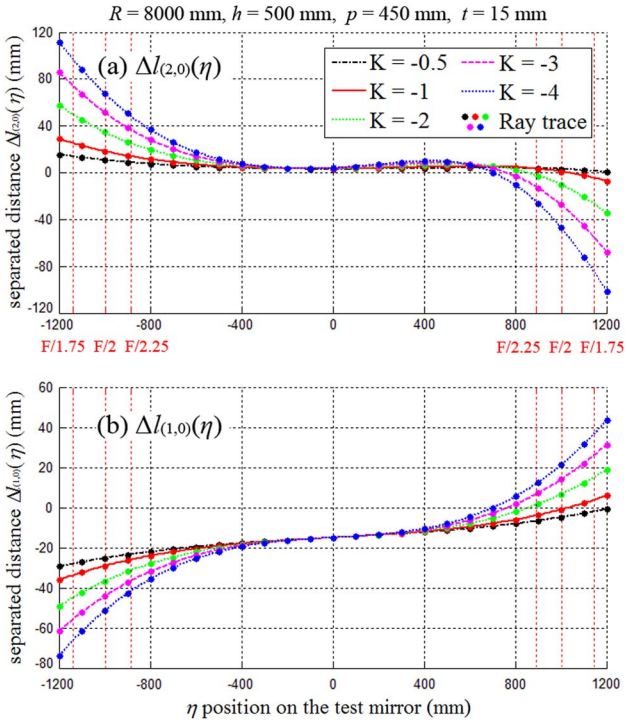

Fig. 3. Influence of the K and $F/\#$ on the separated distances of the orders (2, 0) and (1, 0). The approximate $\Delta l_{(m,0)}(\eta)$ matches the actual one gained by ray trace in Zemax. The nonlinearity of $\Delta l_{(m,0)}(\eta)$ increases as the $F/\#$ decreases or the absolute value of K increases.

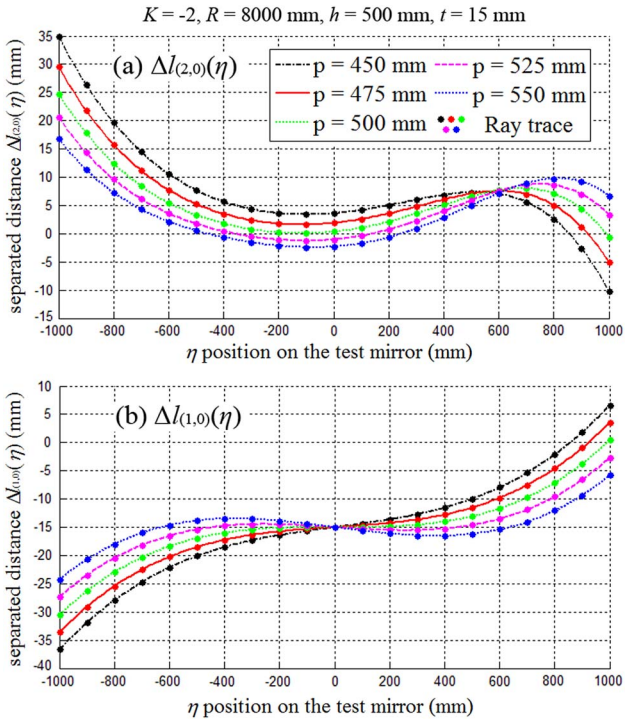

Fig. 4. Separated distance $\Delta l_{(m,0)}(\eta)(m = 1, 2)$ versus the axial distance p between the CGH and the pinhole. The shape of the curve $\Delta l_{(m,0)}(\eta)$ changes like a wave as p varies.

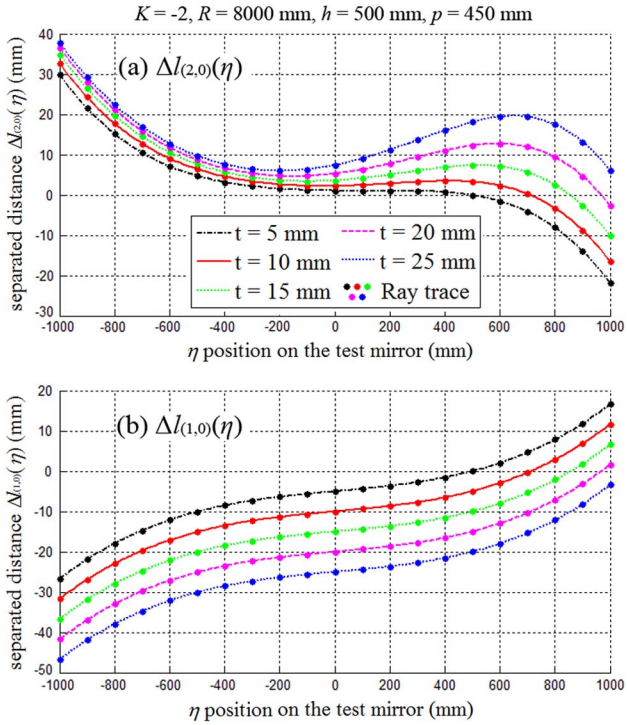

Fig. 5. Separated distance $\Delta l_{(m,0)}(\eta)(m = 1, 2)$ versus the transverse distance t between the CGH and the pinhole. The value of the $\Delta l_{(m,0)}(\eta)$ increases or decreases simultaneously on the $\pm\eta$ axis as t varies.

the shape of the curve $\Delta l_{(m,0)}(\eta)$ changes with a wavelike appearance as the axial distance p varies. Figure 5 indicates that the value of $\Delta l_{(2,0)}(\eta)(\eta > 0)$ is sensitive to the transverse distance t [Fig. 5(a)], which is beneficial to separate the diffraction order (2, 0). Also shown is that the transverse distance t does not affect the shape of the disturbing field of order (1, 0) but changes the relative position between the disturbing field and the pinhole [Fig. 5(b)], which is consistent with Eq. (9).

According to Figs. 3–5, it is easy to find that the condition for separating the order (2, 0) is $\min\{\Delta l_{(2,0)}(\eta)\} \geq L_0$ and that for the order (1, 0) is $\min\{-\Delta l_{(1,0)}(\eta)\} \geq L_0$, where $\min\{\}$ denotes the global minimum. Note that the global minimum of the separated distance of the order (2, 0) is changed from the value of $\Delta l_{(2,0)}(\eta)$ at the boundary of $+\eta$ axis to the local minimum on the $-\eta$ axis when the axial distance p or the transverse distance t is large enough (e.g., $p > 500$ mm or $t \geq 25$ mm).

B. Slight Influence of the CGH Glass Plate

In the parametric model, the CGH glass plate is ignored to derive the expression of the separated distance of the parasitic diffraction orders. However, in practice, the spherical aberration introduced by the CGH glass plate shifts the paraxial focus of the conic mirror.

Supposing the CGH pattern is fabricated on the glass surface toward and distance $(R - h)$ away from the test mirror, the paraxial focus is shifted by a distance Δ, and the filter is placed $(p + \Delta)$ away from the CGH pattern, the error caused by ignoring the CGH glass plate is quantified and illustrated in Fig. 6. Results show that the difference of $\Delta l_{(m,0)}(\eta)$ between

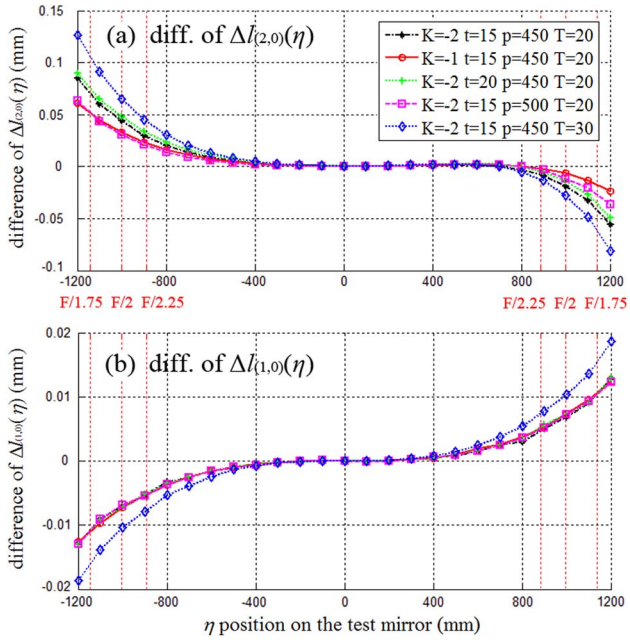

Fig. 6. Influence of the CGH glass plate on $\Delta l_{(m,0)}(\eta)$. The difference is defined as the $\Delta l_{(m,0)}(\eta)$ of the CGH with a glass plate T mm thick minus that of the CGH with a glass plate 0 mm thick. The difference is less than 0.08 mm in the area worthy of consideration, which is small enough to be ignored.

the CGH with and without the glass plate is less than 0.13 mm for the order (2, 0) and 0.02 mm for the order (1, 0), even when the glass plate is thick up to 30 mm. For the order (1, 0), a difference of 0.02 mm is insignificant. For the order (2, 0), only the area where $\min\{\Delta l_{(2,0)}(\eta)\}$ is achieved is worth considering, i.e., the boundary of $+\eta$ axis and the local minimum point on the $-\eta$ axis [Figs. 4(a) and 5(a)]. The difference can be treated as less than 0.08 mm, which is small enough that we can neglect it in optical testing. Therefore, it is reasonable to ignore the influence of the CGH glass plate to construct the parametric model.

C. Diffraction Orders that are Uncertain to be Separated

Only the parasitic diffraction orders (m, n) with $|m| \le 5$ and $|n| \le 5$ are discussed, since the orders higher than 5 have such low diffraction efficiency that they can be ignored. Equation (2) is adopted to analyze whether a given undesired order (m, n) is separable when the orders (2, 0) and (1, 0) are both separated.

Figures 3–5 have showed that $\Delta l_{(2,0)}(\eta) \ge L_0$ and $\Delta l_{(1,0)}(\eta) \le -L_0$ are the condition to separate the orders (2, 0) and (1, 0). Combined with Eq. (2), we obtain

$$p\frac{\partial \Phi}{\partial y} \ge L_0, \qquad 2ph\frac{R-h}{R}\frac{\partial \Phi}{\partial y}\frac{\partial^2 \Phi}{\partial y^2} \le -L_0. \tag{14}$$

According to Eq. (2), when Eq. (14) is held, the undesired orders (m, n) with $(m+n-2)(m-1)(n-1) \le 0$ will be separated, since in this case the two items in Eq. (2) will have the same sign or one of the items is equal to zero. However, the orders (m, n) with $(m+n-2)(m-1)(n-1) > 0$ are uncertain to be separated because of the neutralization of the two items.

All the diffraction orders (m, n) are listed in Fig. 7. The parasitic orders (m, n) with $(m+n-2)(m-1)(n-1) = 0$ are marked in light green, and those with $(m+n-2)(m-1)(n-1) < 0$ are marked in blue. Both of them are separated. The orders with $(m+n-2)(m-1)(n-1) > 0$ are marked in yellow and white, where those marked in yellow are usually separated because parts or most of their stray rays are beyond the apertures of the test mirror and the CGH. Therefore, only the orders marked in white are uncertain to be separated.

The ratio of the total diffraction efficiency of the uncertain orders (marked in white) to that of the desired order (1, 1) is concentrated on. Since CGHs are usually made with a duty cycle of 0.5 and a fringe position error of 0.1 μm is achievable currently [15,16], it is reasonable to assume that the practical duty cycle is between 0.475 and 0.525 for a CGH with a line spacing of 5–30 μm. For ideal chrome-on-glass CGHs or phase-type CGHs with different duty cycles and etching depths [15], the ratio is listed in Table 1. Results show that when the duty cycle is between 0.475 and 0.525, the ratio is less than 5.09%, which is small enough to be ignored in practical optical testing. Besides, in most cases, not all of the uncertain orders are unseparated. Therefore, a slight influence of the uncertain orders is guaranteed and can be neglected.

4. OPTIMAL DESIGN

Reducing the carrier frequency to increase the line spacing to alleviate the manufacturing constraints, and maintaining an acceptable size and a tolerable mapping distortion are the goals of CGH design. For a practical test mirror, the curvature R, the f-number, and the conic constant K are specified. The size and the mapping distortion of the CGH, which are fully determined by the distance h between the CGH and the paraxial focus shown in Section 2.A, are usually traded off and fixed

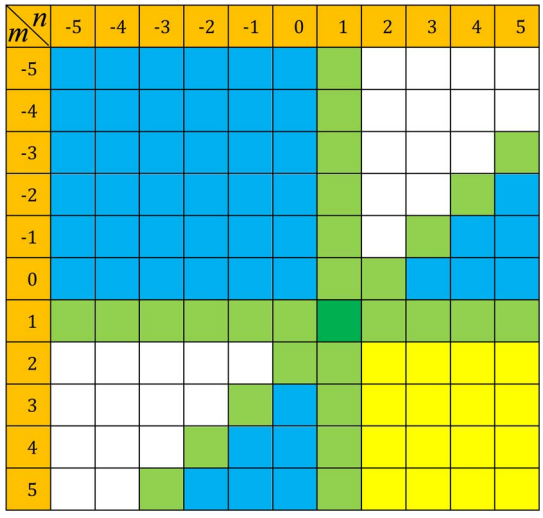

Fig. 7. Entire diffraction orders (m, n) with $|m| \le 5$ and $|n| \le 5$ of a CGH when the orders (2, 0) and (1, 0) are both separated. The order marked in dark green is the desired one. The orders marked in white are uncertain to be separated. Orders marked in the other colors are separable.

Table 1. Total Diffraction Efficiency of the Uncertain Orders Compared to that of the Desired Order

CGH Type	Duty Cycle	Etching Depth	Ratio (%)
Chrome-on-glass	0.5	–	3.68
Chrome-on-glass	0.475, 0.525	–	5.09
phase	0.5	0.5, 0.475, 0.525	3.68
phase	0.475, 0.525	0.5, 0.475, 0.525	5.09

at the beginning of design. Thus, searching for the most apposite axial distance p and transverse distance t between the CGH and the pinhole, i.e., the parameters (p, t), is the goal if a suitable parameter h has been adopted to meet the requirements of the size and the mapping distortion.

Given a 2 m diameter hyperboloid with $K = -2$ and $F/\# = 2$ is under test and the parameter h is chosen as 500 mm, the parameters (p, t) are attained by the following steps:

(1) Permitted range of p and t determined by the order (2, 0)

For the diffraction order (2, 0), the inequality $\min\{\Delta l_{(2,0)}(\eta)\} \geq L_0$ determines the allowed range of the parameters (p, t), i.e., the axial distance p and the transverse distance t between the CGH and the pinhole. The $\min\{\Delta l_{(2,0)}(\eta)\}$ versus p and t is illustrated in Fig. 8. The noticeable broken lines in the contour lines are caused by the fact that the value of the $\min\{\Delta l_{(2,0)}(\eta)\}$ shifts from the point at the periphery of the test mirror to the local minimum point around the center, explained in Section 3.A. The permitted range, i.e., the upper left region delimited by the contour lines, decreases along the direction of the $+t$ axis and the $-p$ axis as L_0 increases. The area with the contour lines lower than $L_0 (L_0 > 0)$ is forbidden for the parameters (p, t), where parts of the stray rays are irremovable.

(2) Permitted range of p and t determined by the order (1, 0)

For the diffraction order (1, 0), the contour lines of the $\min\{-\Delta l_{(1,0)}(\eta)\}$ are plotted in Fig. 9 with an increment of 1.0 mm. Unlike Fig. 8, there are no broken lines in Fig. 9, since the value of the $\min\{-\Delta l_{(1,0)}(\eta)\}$ is always achieved at the periphery of the test mirror as long as the filter plane is settled inside the point with the least blur circle[7].

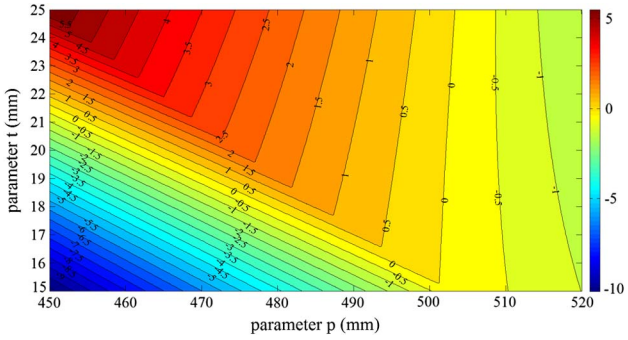

Fig. 8. Contour lines of $\Delta l_{(2,0)}(\eta)$ with an increment of 0.5 mm in the $p - t$ plane. The upper left region with contour lines larger than L_0 (e.g., $L_0 = 0.5$ mm) is the permitted range for (p, t). ($K = -2$, $F/\# = 2$, $R = 8000$ mm, and $h = 500$ mm.)

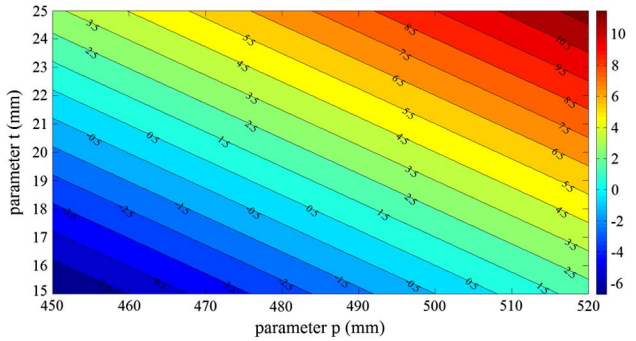

Fig. 9. Contour lines of $\Delta l_{(1,0)}(\eta)$ with an increment of 1.0 mm in the $p - t$ plane. The upper right region with contour lines larger than L_0 (e.g., $L_0 = 0.5$ mm) is the permitted range for (p, t). ($K = -2$, $F/\# = 2$, $R = 8000$ mm, and $h = 500$ mm.)

(3) Merit function versus the parameter p and t

Qualitative analysis: The CGH with tilt carriers still has a certain power. The amount of tilt carrier frequency is determined by t/p, while the amount of power carrier frequency is determined by $|1/h - 1/p|$ [13]. Therefore, the optimal design is achieved when the lowes values of t/p and $|1/h - 1/p|$ are attained in the permitted range of p and t.

Quantitative analysis: The line spacing of CGH limits the accuracy of fabrication. For the sake of insuring the low risk of fabrication errors, we choose the valley value of the local line spacing on the meridional plane as a merit function. The combination (p, t) within the final permitted range, i.e., the intersection of the permitted ranges obtained in steps (1) and (2), which achieves the greatest value of the merit function is defined as the optimal design.

The local line spacing s on the meridional plane is calculated as [7]

$$s = \lambda \Big/ \left| \frac{\partial \Phi}{\partial y} \right|, \tag{15}$$

where $\lambda = 0.6328$ μm is the working wavelength of the interferometer, and $\partial\Phi/\partial y$ is gained in Eq. (4).

The merit function in the $p - t$ plane is plotted in Fig. 10 as the background, where (p, t) are the axial distance and transverse distance between the CGH and the pinhole, respectively. The value of the merit function increases along the direction from upper left to lower right. The final permitted range is the upper left area demarcated by the broken contour lines denoted with the different criterion L_0. Given an L_0, the optimal design, i.e., the most apposite (p, t) that achieves the greatest value of the merit function, is located at the corner of the boundary of the corresponding final permitted range and marked with a red circle. For example, if $L_0 = 0.5$ mm, the optimal design is $(p, t) = (493.8$ mm, 16.75 mm).

It must be emphasized that the merit function can be chosen arbitrarily as long as it denotes the level of the line spacing of a CGH, e.g., the mean value of the local line spacing. Besides, the optimal design might shift slightly along the contour line versus different merit functions when the corner of the boundary of the final permitted range is blunt like a circle.

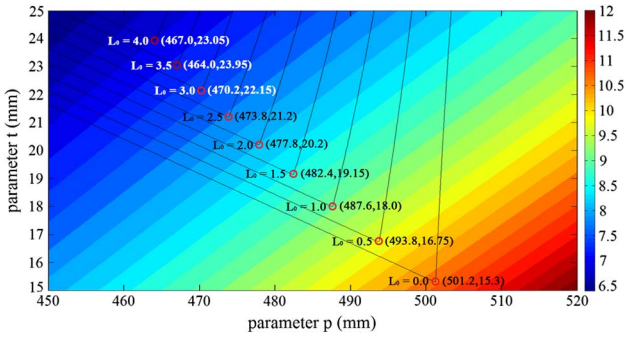

Fig. 10. Merit function in the $p - t$ plane and the optimal designs of (p, t). The optimal designs of (p, t) for the different criterion L_0 are marked with red circles and located at the corners of contour lines. ($K = -2$, $F/\# = 2$, $R = 8000$ mm, and $h = 500$ mm.)

The optimal design is affected by the conic constant K. Assuming a series of 2 m diameter $F/2$ conic surfaces with different K under test, the distance h between the CGH and the paraxial focus is settled as 500 mm, and the criterion $L_0 = 0.5$ mm, the final permitted range of the axial distance p and transverse distance t between the CGH and the pinhole and the optimal design versus the K are illustrated in Fig. 11. Analogously, for a given conic constant K, the permitted range is the upper left area delimited by the corresponding broken lines. All the optimal designs are located at the corners of the contour lines. Note that the optimal design shifts along the $+p$ axis and $+t$ axis as the absolute value of K increases.

Admittedly, the f-number of the test mirror also affects the optimal design. If a series of paraboloids with different f-numbers are under test, $R = 8000$ mm, $h = 500$ mm, and $L_0 = 0.5$ mm, the final permitted ranges and optimal designs are exhibited and marked with red circles in Fig. 12. Results show that for different f-numbers, the Dexter boundaries of the final permitted ranges coincide. So all the optimal designs lie on the same curve. The reason is that the curve denotes the contour line of the value of the local minimum point on the $-\eta$ axis versus p and t, which is not affected by f-number.

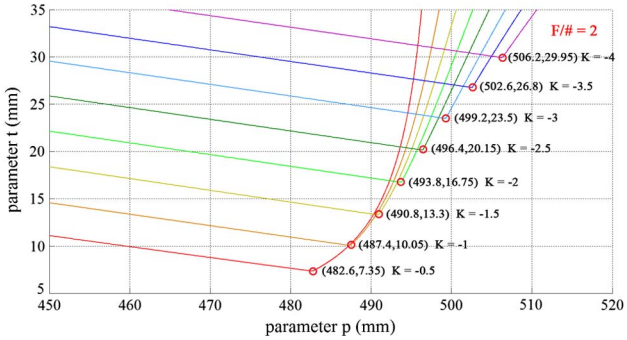

Fig. 11. Final permitted ranges and optimal designs for conic surfaces with diverse K and identical $F/\#$. For a given K, the permitted range is the upper left area demarcated by the corresponding broken lines, and the optimal design is located in the corner and marked with a red circle. ($F/\# = 2$, $R = 8000$ mm, $h = 500$ mm and $L_0 = 0.5$ mm.)

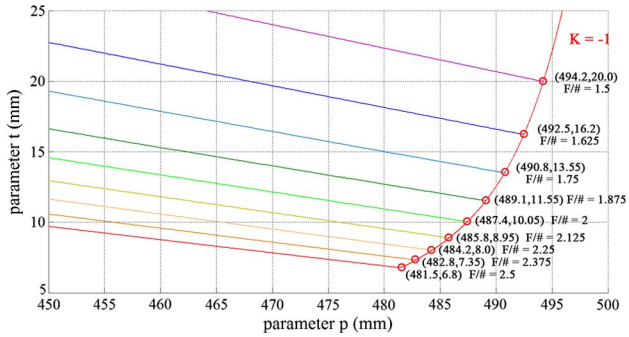

Fig. 12. Final permitted ranges and optimal designs for conic surfaces with diverse $F/\#$ and identical K. The Dexter boundaries of the final permitted ranges coincide, and all the optimal designs lie on the same curve. ($K = -1$, $R = 8000$ mm, $h = 500$ mm, and $L_0 = 0.5$ mm.)

5. CGH DESIGN EXAMPLES

In the parametric model, we only concentrate on the diffraction orders (2, 0) and (1, 0) as the representative parasitic orders to deduce the optimal design. The following examples are designed with the optimal design method to confirm its application.

A. Examples of Conic Surfaces

The Hubble Space Telescope primary mirror is an $F/2.3$ quasi-paraboloid with $K = -1.0022985$ [17]. If the primary mirror is tested as a mirror with no central hole, the criterion L_0 is 0.5 mm, and the distance h between the CGH and the paraxial focus is settled as 620 mm to achieve a CGH with a size of about 149 mm (main CGH section) and an acceptable mapping distortion, the optimal design is attained by the steps presented in Section 4 as $(p, t) = (603.8\text{ mm}, 9.65\text{ mm})$. The corresponding CGH is designed with Zemax, as shown in Fig. 13(a). The valley value of the local line spacing is 21.21 μm, consistent with 21.12 μm calculated with the parametric model. The minute difference is resulted in by the spherical aberration introduced by the CGH glass plate.

Typical orders are shown in Fig. 13(b). All the parasitic orders are separated except the seventeen orders (−5, 4), (4, −5), (−5, 3), (3, −5), (−4, 4), (4, −4), (−4, 3), (3, −4), (−3, 4), (−3, 3), (3, −3), (−2, 3), (3, −2), (−2, 2), (2, −2), (−1, 2), and (2, −1). When the duty cycle is between 0.475 and 0.525, the ratio of the total diffraction efficiency of the unseparated orders to that

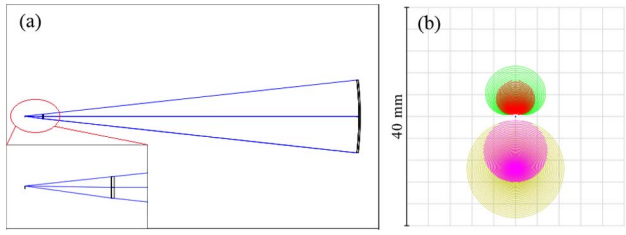

Fig. 13. (a) CGH null test design for the Hubble primary mirror. The CGH pattern is fabricated on the right plane of the 20.0 mm thick BK7 glass substrate. (b) Typical disturbing orders are separated: 0.50 mm for the order (0, 2) (red), 0.50 mm for the order (2, 0) (green), 0.78 mm for the order (0, 1) (purple), and 0.78 mm for the order (1, 0) (brown).

of the desired order (1, 1) is less than 4.57%, which is small enough that we can ignore it in practical optical testing.

Consider that a 1 m diameter $F/2$ hyperboloid with $K = -2$ is under test, and $L_0 = 0.5$ mm. If the distance h between the CGH and the paraxial focus is chosen as 250 mm, according to Eq. (11) and Fig. 10, the optimal design for (p, t) is (487.6/2 mm, 18.0/2 mm) = (243.8 mm, 9.0 mm). The corresponding CGH is designed with a size of about 77.5 mm and a valley value of the local line spacing of 9.20 μm, approximate to 9.17 μm obtained in Eq. (15). The BK7 glass plate is 10.0 mm thick. The separated distances of the typical disturbing diffraction orders are 0.47 mm for the order (0, 2), 0.50 mm for the order (2, 0), 0.51 mm for the order (0, 1), and 0.51 mm for the order (1, 0). The least separated distance is 0.47 mm, which is close to L_0 and hence acceptable. Similarly, parts of the parasitic orders are not separated. They are the orders (−5, 3), (3, −5), (−5, 2), (2, −5), (−4, 3), (3, −4), (−4, 2), (2, −4), (−3, 3), (3, −3), (−3, 2), (2, −3), (−2, 3), (−2, 2), (2, −2), (−1, 2), and (2, −1). The ratio of the total diffraction efficiency of the unseparated orders to that of the desired order (1, 1) is also less than 4.57%, which is small enough to be neglected, when the duty cycle is between 0.475 and 0.525.

The optimal designs of CGHs for the conic mirrors with $-4 \le K < 0$ and $1.5 \le F/\# \le 2.5$ are discussed in Section 4. In order to define the application range of the parametric model or the optimal design method, the extreme case, $K = -4$ and $F/\# = 1.5$, is considered. Assuming that a 1 m diameter $F/1.5$ hyperboloid with $K = -4$ is under test, with $L_0 = 0.5$ mm and $h = 400$ mm, the optimal design is gained as $(p, t) = (399.2$ mm, 26.8 mm). The CGH is designed with a size of about 180 mm (main CGH section), and typical stray diffraction orders are separated, as shown in Fig. 14. The valley value of the local line spacing is 5.15 μm, which is close to 5.14 μm obtained with the parametric model. The fourteen orders (−5, 3), (3, −5), (−5, 2), (2, −5), (−4, 3), (3, −4), (−4, 2), (2, −4), (−3, 2), (2, −3), (−2, 2), (2, −2), (−1, 2), and (2, −1) are not separated. The ratio is less than 2.27% when the duty cycle is between 0.475 and 0.525, which is small enough to be ignored. Results indicate that the optimal design method shows good applicability when $K = -4$ and $F/\# = 1.5$.

B. Examples of Surfaces with Aspheric Coefficients

Assuming a 2 m diameter $F/1.7$ ellipsoid with $K = -0.97$, $R = 6800$ mm, the fourth-order to eighth-order coefficients $A = 0$ mm^{-3}, $B = 9.81 \times 10^{-24}$ mm^{-5}, and $C = -5.92 \times 10^{-30}$ mm^{-7} under test, the criterion $L_0 = 0.5$ mm, and the distance h between the CGH and the paraxial focus chosen as 250 mm to gain a CGH with a main section of less than 95.0 mm, the optimal design is gained as $(p, t) = (245.8$ mm, 11.65 mm). The valley value of the local line spacing is 7.25 μm, in accordance with 7.23 μm obtained with the parametric model. The BK7 glass plate is 12.0 mm thick. Typical parasitic diffraction orders are separated: 0.48 mm for the order (0, 2), 0.51 mm for the order (2, 0), 0.54 mm for the order (0, 1), and 0.53 mm for the order (1, 0). The least separated distance is 0.48 mm, which is close to the criterion $L_0 = 0.5$ mm. Parts of the parasitic orders are not separated. They are the orders (−5, 3), (3, −5), (−5, 2), (2, −5), (−4, 3), (3, −4), (−4, 2), (2, −4), (−3, 3), (3, −3), (−3, 2), (2, −3), (−2, 2), (2, −2), (−1, 2), and (2, −1). When the duty cycle is between 0.475 and 0.525, the ratio of the total diffraction efficiency of the unseparated orders to that of the desired order (1, 1) is less than 4.51%, which is small enough to be ignored.

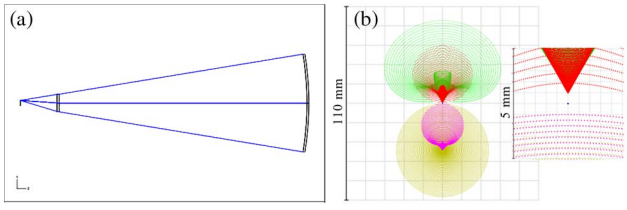

Fig. 14. (a) Design of a CGH used for the 1 m diameter $F/1.5$ hyperboloid with $K = -4$. The BK7 glass plate is 24 mm thick. (b) Typical parasitic diffraction orders are separated: 0.49 mm for the order (0, 2) (red), 0.51 mm for the order (2, 0) (green), 0.50 mm for the order (0, 1) (purple), and 0.50 mm for the order (1, 0) (brown).

5. CONCLUSION

CGHs with tilt carrier frequencies placed outside the interferometer focus used for testing the concave aspherics are investigated in this paper. As further research of our previous work, we have expanded the application range of the parametric model from $-0.5 \le K < 0$ and $F/\# \ge 2$ to $-4 \le K < 0$ and $F/\# \ge 1.5$ by concentrating on the representative orders (2, 0) and (1, 0) and deriving all the expressions up to seventh order based on the mirror coordinate without paraxial approximation.

An optimal design method has been proposed in this paper by using the parametric model. It has two advantages: (1) separating the parasitic diffraction orders [unseparated orders have such a low diffraction efficiency compared to that of the desired order (1, 1) that they can be ignored] and (2) achieving the largest line spacing to reduce the risk of fabrication. This approach solves the problem of laborsome manual operation of the trial and error method to design an appropriate and practicable CGH.

The procedure of the optimal design method can be described as below.

- Choose a suitable distance from the CGH to the paraxial focus of the test mirror to satisfy the requirement of the size and the mapping distortion.
- Estimate the necessary separated distance based on the practical precision of fabrication and alignment of the pinhole.
- Calculate the permitted range of the axial and transverse distances between the CGH and the pinhole determined by the representative orders (2, 0) and (1, 0).
- Plot the merit function that denotes the level of the line spacing, combined with the permitted range, to find the optimal solution for the axial and transverse distances between the CGH and the pinhole.

Acknowledgment. We are grateful to the anonymous reviewers for their detailed comments and valuable suggestions which helped to improve the quality of this paper.

REFERENCES

1. A. J. MacGovern and J. C. Wyant, "Computer generated holograms for testing optical elements," Appl. Opt. **10**, 619–624 (1971).

2. H. P. Stahl, "Aspheric surface testing techniques," Proc. SPIE **1332**, 66–76 (1990).
3. D. Malacara, *Optical Shop Testing*, 3rd ed., Vol. **59** of Wiley Series in Pure and Applied Optics (Wiley, 2007).
4. Z. Gao, M. Kong, R. Zhu, and L. Chen, "Problems on design of computer-generated holograms for testing aspheric surfaces: principle and calculation," Chin. Opt. Lett. **5**, 241–244 (2007).
5. S. Peterhänsel, C. Pruss, and W. Osten, "Phase errors in high line density CGH used for aspheric testing: beyond scalar approximation," Opt. Express **21**, 11638–11651 (2013).
6. M. Novak, C. Zhao, and J. H. Burge, "Distortion mapping correction in aspheric null testing," Proc. SPIE **7063**, 706313 (2008).
7. Y. C. Chang, "Diffraction wavefront analysis of computer-generated holograms," Ph.D. thesis (University of Arizona, 1999).
8. G. S. Khan, K. Mantel, I. Harder, N. Lindlein, and J. Schwider, "Design considerations for the absolute testing approach of aspherics using combined diffractive optical elements," Appl. Opt. **46**, 7040–7048 (2007).
9. P. Zhou, W. Cai, C. Zhao, and J. H. Burge, "Parametric definition for the CGH patterns and error analysis in interferometric measurements," Proc. SPIE **8415**, 841505 (2012).
10. W. Cai, P. Zhou, C. Zhao, and J. H. Burge, "Diffractive optics calibrator: measurement of etching variations for binary computer-generated holograms," Appl. Opt. **53**, 2477–2486 (2014).
11. N. Lindlein, "Analysis of the disturbing diffraction orders of computer-generated holograms used for testing optical aspherics," Appl. Opt. **40**, 2698–2708 (2001).
12. E. Garbusi and W. Osten, "Analytical study of disturbing diffraction orders in in-line computer generated holograms for aspheric testing," Opt. Commun. **283**, 2651–2656 (2010).
13. J. Peng, J. Ren, X. Zhang, and Z. Chen, "Analytical investigation of the parasitic diffraction orders of tilt carrier frequency computer-generated holograms," Appl. Opt. **54**, 4033–4041 (2015).
14. W. T. Welford, "A vector raytracing equation for hologram lenses of arbitrary shape," Opt. Commun. **14**, 322–323 (1975).
15. P. Zhou, J. H. Burge, and S. Peterhansel, "Optimal design of computer-generated holograms to minimize sensitivity to fabrication errors," Opt. Express **15**, 15410–15417 (2007).
16. J. C. Wyant, "Computerized interferometric surface measurements," Appl. Opt. **52**, 1–8 (2013).
17. L. A. Montagnino, "Test and evaluation of the Hubble space telescope 2.4-meter primary mirror," Proc. SPIE **571**, 182–190 (1985).